Biomaterials 89 (2016) 14–24

Contents lists available at ScienceDirect

Biomaterials

journal homepage: www.elsevier.com/locate/biomaterials

Matrix stiffness modulates formation and activity of neuronal networks of controlled architectures

Joséphine Lantoine [a], Thomas Grevesse [a], Agnès Villers [b], Geoffrey Delhaye [a], Camille Mestdagh [a], Marie Versaevel [a], Danahe Mohammed [a], Céline Bruyère [a], Laura Alaimo [a], Stéphanie P. Lacour [c], Laurence Ris [b], Sylvain Gabriele [a, *]

[a] Mechanobiology & Soft Matter Group, Laboratoire Interfaces et Fluides Complexes, Centre d'Innovation et de Recherche en Matériaux Polymères (CIRMAP), Research Institute for Biosciences, Université de Mons, 20, Place du Parc, B-7000 Mons, Belgium
[b] Department of Neuroscience, University of Mons, Belgium
[c] Laboratory for Soft Bioelectronics Interfaces, Centre for Neuroprosthetics, Ecole Fédérale Polytechnique de Lausanne, Switzerland

ARTICLE INFO

Article history:
Received 2 January 2016
Received in revised form
14 February 2016
Accepted 23 February 2016
Available online 26 February 2016

Keywords:
Neuronal networks
Matrix stiffness
Micropatterning
Migration
Mechanotaxis

ABSTRACT

The ability to construct easily *in vitro* networks of primary neurons organized with imposed topologies is required for neural tissue engineering as well as for the development of neuronal interfaces with desirable characteristics. However, accumulating evidence suggests that the mechanical properties of the culture matrix can modulate important neuronal functions such as growth, extension, branching and activity. Here we designed robust and reproducible laminin-polylysine grid micropatterns on cell culture substrates that have similar biochemical properties but a 100-fold difference in Young's modulus to investigate the role of the matrix rigidity on the formation and activity of cortical neuronal networks. We found that cell bodies of primary cortical neurons gradually accumulate in circular islands, whereas axonal extensions spread on linear tracks to connect circular islands. Our findings indicate that migration of cortical neurons is enhanced on soft substrates, leading to a faster formation of neuronal networks. Furthermore, the pre-synaptic density was two times higher on stiff substrates and consistently the number of action potentials and miniature synaptic currents was enhanced on stiff substrates. Taken together, our results provide compelling evidence to indicate that matrix stiffness is a key parameter to modulate the growth dynamics, synaptic density and electrophysiological activity of cortical neuronal networks, thus providing useful information on scaffold design for neural tissue engineering.

1. Introduction

Mechanical cues from the extracellular matrix (ECM) are implicated in a variety of biological processes and pathological situations of the nervous system [1]. Soft matrices have been found to promote neurite outgrowth and axon specification [2,3], whereas more rigid substrates lead to increased dendrite number and branching [4]. In a pathological context, degenerative disease or brain injury may imply significant modifications of the local or global stiffness of brain tissues. Indeed, magnetic resonance elastography (MRE) examinations of brain tissues has shown significantly reduced brain tissue stiffness in patients with Alzheimer's disease [5], whereas emerging evidence suggest that local tissues stiffness is likely to increase after injury. In addition, the immature brain was reported to be approximately twice as stiff as adult brain of pig [6] or rats [7], suggesting that a larger amount of force is required to deform the pediatric brain compared to the adult one. Taken together, these observations have led to recognition of the ECM mechanical properties as an important parameter in understanding physiological and pathological situations, as well as designing innovative scaffolds for tissue engineering. However, information about the influence of the matrix rigidity on neuronal network assembly and function is still lacking.

To address this problem, a promising *in vitro* approach consists in studying the assembly of living networks with imposed topologies and their functional activity [8,9]. However, this approach requires to control the spatial confinement of neuronal structures on culture matrices with tunable rigidities. In this work, we created cortical neuronal cultures of controlled architectures by coupling a

* Corresponding author.
E-mail address: sylvain.gabriele@umons.ac.be (S. Gabriele).

http://dx.doi.org/10.1016/j.biomaterials.2016.02.041
0142-9612/

microcontact printing of ECM protein with two polymeric matrices that have a 100-fold difference in Young's modulus and investigated the growth, maturation and electrophysiological behavior of cortical neuronal networks.

2. Method

2.1. Preparation and characterization of culture substrates

Stiff substrates of ~500 kPa in Young's modulus were made in polydimethylsiloxane (PDMS), which has been increasingly employed for the fabrication of neuronal cell culture platforms [10] and microfluidic devices [11]. PDMS curing agent (Dow Corning, Sylgard 184) was mixed with a base agent in a mass ratio of 22:1 in 15 ml centrifugal tubes [12]. The mixture was placed in a vacuum for 30 min to remove air bubbles and a volume of 100 μl was transferred using a micropipette onto the top of a 25 mm glass coverslip. Then the PDMS mixture was spin-coated at 5000 rpm for 20 s and cured at 60 °C for 4 h. Samples were stored at room temperature in a vacuum desiccator.

Soft substrates of ~5 kPa in Young's modulus were made by mixing acrylamide (AAm, A8887, Sigma) and bisacrylamide (bis-AAm, 146072,Sigma) with N-hydroxyethylacrylamide monomers (HEA, 697931,Sigma) to form a hydrophilic network of polyacrylamide with hydroxyl groups (hydroxy-PAAm), as previously described [13,14].

The Young's moduli of PDMS elastomers and hydroxy-PAAm hydrogels were measured by DMA (Dynamic Mechanical Analysis, Mettler Toledo DMA/SDTA 861e, Switzerland) at 37 °C in compression mode on circular cylindrical samples of 15 mm in diameter and height of 10 mm. Samples were sandwiched between two parallel plates and an oscillating strain of maximum amplitude of 10% was applied and the stress needed to deform the cylindrical samples was measured over a frequency range of 0.1–10 Hz. During compression testing, a settling time of approximately one minute was used to achieve a stable measurement of the storage modulus at each frequency. We obtained a Young's modulus of 508 ± 16 kPa for stiff PDMS ($n = 13$), 5.0 ± 0.3 kPa for soft hydroxy-PAAm ($n = 14$) and 425 ± 18 kPa ($n = 12$) for stiff hydroxy-PAAm.

2.2. Microcontact printing

To ensure a similar biochemical surface functionalization of both culture matrices, soft and stiff substrates were micropatterned with a mix solution of poly-L-lysine (PLL, P4707, Sigma) and laminin (LM, L2020,Sigma). LM and PLL densities were determined on both substrates by immunofluorescence detection of labeled LM and PLL. We found a constant fluorescence intensity level across the different materials indicating uniform distribution of ligand density and no statistical differences of protein density were found between both matrices (Fig. S1).

Flat PDMS microstamps were prepared by casting a 10:1 (w/w) degassed mixture of PDMS prepolymer and curing agent (Sylgard 184, Dow Corning) on a silicon wafer, which was passivated with fluorosilane (tridecafluoro-1,1,2,2-tetrahydrooctyl-1-trichlorosilane, Gelest) in a vacuum to facilitate the removal of the PDMS layer. After curing overnight at 65 °C, flat PDMS microstamps were peeled off the silicon master, washed with ethanol and made hydrophilic by exposure to ultraviolet-ozone (UV/O_3). Activated PDMS microstamps were incubated with a sterile solution of PLL-LM for 1 h at room temperature then dried with pure nitrogen. Inked PDMS microstamps were then gently applied on soft and stiff matrices. Uncoated regions were blocked by incubating PDMS substrates for 5 min in a 1% Pluronic F-127 solution (BASF, Mount Olive, NJ) and hydroxy-PAAm hydrogels during one night at 4 °C in a Bovine Serum Albumine (BSA) solution (5 mg/ml in PBS). After blocking, both substrates were washed three times with a sterile PBS solution.

2.3. Cell culture

Primary rat cortical neurons (RCN) prepared from the cortex of day-18 rat embryos (A10840-01, Life Technologies, Gaithersburg, MD) were suspended in a culture medium (21103-049, Neurobasal Medium, Life Science) supplemented with B-27, 1% antibiotic (15140-122, Life Technologies), 5 ml GlutaMAX-I (35050-061, Life Technologies) and 50 μl of nerve growth factor (0.01 μg/ml,556-NG, R&D systems). Each culture corresponded to approximately 1.3 million cortical neurons obtained from 2 day-18 rat embryos. RCN were seeded on microprinted substrates at a density of 50,000 cells per cm^2 and incubated under standard conditions at 37 °C and 5% CO_2. Media was replaced the day after the seeding and then every 48 h until experiments were executed. Experiments were performed on either 6 h after seeding (DIV0) and at days 4 (DIV4), 9 (DIV9) or 15 (DIV15) post seeding.

2.4. Pharmacological agents

In one experiment, a concentration of 0.3 nM of Nocodazole (M1404, Sigma–Aldrich) was used during three days after the seeding to inhibit the polymerization of microtubules [15]. Immunofluorescent staining of ß-III tubulin was performed at DIV4 for assessing the correct microtubule inhibition.

2.5. Cell viability

Live/Dead assays were performed with Sytox Green (S7020, Life Technologies) to visualize dead cells and Hoechst:33342 (62249, Invitrogen) to stain live and dead cells. Cells were incubated during 15 min at 37 °C with 10 μl of Sytox Green (1 μM) diluted in 2 ml of neurobasal medium complemented with 50 μL of Hepes (SH30237.01, Hyclone), rinsed with warm PBS and fixed with paraformaldehyde 4% (Electron Microscopy) during 10 min. Cells were labeled with Hoechst:33342 (1:200) during 45 min at 37 °C. After three washes with PBS, stained cells were mounted on microscope glass slides with Slow Fade Gold Antifade (Molecular Probes, Life Technologies).

2.6. Immunocytochemistry

For labeling microtubules, actin filaments and the nucleus, RCN were permeabilized for 1 min with a solution of 0.25% glutaraldehyde (Electron Microscopy Sciences, Hatfield, PA) and fixed with 0.5% Triton X-100 (Sigma) in cytoskeletal buffer (CB). A second incubation with 1% glutaraldehyde in CB was then performed for 10 min. After three washes, RCN were labeled with a primary antibody (anti-beta tubulin antibody produced in mouse, 1:200, T5293, Sigma) for staining microtubules, phalloidin conjugated with alexa fluor 488 (1:200, A12379, Invitrogen) for staining F-actin and DAPI (1:200, Invitrogen) to visualize the nuclei. A second incubation with a secondary antibody tetramethylrhodamine-labeled (goat anti-mouse 1:200, Sigma) was performed. Coverslips were mounted on microscope glass slides with Slow Fade Gold Antifade (Molecular Probes, Invitrogen).

For labeling synaptic vesicle proteins, cells were fixed with paraformaldehyde 4% in PBS for 10 min and permeabilized with 0.02% Triton X100 in PBS for 10 min. Then cells were incubated with a blocking solution containing 5% BSA in PBS. After three washes, cells were labeled with anti-synapsin conjugated for staining synapsin (1:600, 106 011C3, Synaptic Systems), anti-βIII-tubulin alexa

fluor 488 conjugated for staining microtubules (1:300, AB15708A4, Millipore) and DAPI for one night at 4 °C. Coverslips were mounted on microscope glass slides with Slow Fade Gold Antifade (Molecular Probes, Invitrogen).

For labeling MAP-2 and Tau proteins, primary cortical neurons were fixed with paraformaldehyde (#P6148, Sigma–Aldrich) 4% supplemented with Sucrose 4% (#S7903, Sigma–Aldrich) in PBS for 10 min and permeabilized with 0.3% Triton X-100 (#T8787-250ML, Sigma–Aldrich) in warm PBS for 5 min. Then cells were incubated in a blocking solution with 5% BSA in PBS. After three washes in PBS, cortical neurons were labeled with anti-MAP2 antibody (1:250, #M3696, Sigma–Aldrich), anti-TAU (1:500, MAB3420, Millipore) and DAPI (#D1306, ThermoFisher Scientific) for 1 h at room temperature. Incubation with secondary antibodies tetramethylrhodamine goat anti-mouse (1:250, #T2762, Invitrogen) and sheep anti-rabbit FITC (1:250, #F7512, Sigma–Aldrich) was performed during 1 h at room temperature. Coverslips were mounted on microscope glass slides with SlowFade Gold Antifade (#S36936, Thermofisher Scientific).

2.7. Epifluorescent and confocal imaging

Immunostained preparations were observed in epifluorescence and confocal mode with an inverted Nikon Eclipse Ti-E motorized microscope (Nikon, Japan) equipped with × 10 Plan Apo (NA 1.45), × 40 Plan Apo (NA 1.45, oil immersion) and × 60 Plan Apo (NA 1.45, oil immersion) objectives, two lasers (Ar-ion 488 nm; HeNe, 543 nm) and a modulable diode (408 nm). Epifluorescence images were captured with a Roper QuantEM: 512SC EMCCD camera (Photometrics, Tucson, AZ) using NIS Elements AR (Nikon, Japan) and confocal images were acquired with a Nikon C1 scanhead.

2.8. Fluorescence measurement

Soft hydroxy-PAAm (E~5 kPa) and stiff PDMS (E~500 kPa) substrates were microprinted with PDMS microstamps incubated during 1 h at room temperature with labeled laminin (rhodamine laminin, Cytoskeleton Inc, LMN01-A). Microprinted substrates were imaged in epifluorescence mode with a Nikon Eclipse Ti-E motorized inverted microscope equipped with a × 10 Plan Apo objective, a pre-centered illumination system (Intensillight, Nikon, Japan) and a Roper QuantEM:512SC EMCCD camera (Photometrics Tucson, AZ). All images were taken with NIS-Elements Advanced Research software (v. 4.5, Nikon, Japan) using similar illumination and recording conditions (camera frequency, gain, and lamp intensity). The micropattern outline was automatically detected in NIS Elements using a mask obtained from a thresholded image. The micropattern area, the raw integrated density and the mean gray value was the measured for each fluorescent micropattern. In addition, five random background regions were selected near the fluorescent micropattern to obtain a mean gray value of the fluorescent background. The corrected micropattern fluorescence was calculated using the following relation: corrected micropattern fluorescence = raw integrated density − (micropattern area * mean fluorescence background).

MAP-2/Tau images on soft and stiff substrates are averaged images obtained from different areas (soft: n = 14 and stiff: n = 12) using a total of 5 different cultures. Fluorescent MAP-2 and Tau images were first translated in NIS Elements software to ensure a perfect superposition and then MAP-2 and Tau averaged images was produced. The quantification of the ratio of synapsin area to tubulin area was performed in NIS Elements Advanced Research (v4.5, Nikon, Japan) with n = 16 (soft) and n = 15 (stiff) areas obtained from 5 different cultures.

2.9. Patch clamp measurements and analysis

Neuronal networks grown on stiff and soft matrices were incubated at room temperature in submerged recording chamber mounted on an inverted phase contrast microscope (Olympus IX70). Extracellular solution was perfused at a rate of 1 ml/min and contained (in mM): 145 NaCl, 3 KCl, 2 MgCl2, 2 CaCl2, 10 D-Glucose, 15 Hepes and 0.001 glycine, adjusted to pH 7.4 with NaOH. Recording electrodes (4–7 MΩ tip resistance) were pulled from filamented borosilicate glass capillaries (GC150F-10, Harvard Apparatus) by means of a horizontal pipette puller (P-97 Micropipette Puller, Sutter Instruments) and filled with an internal solution containing (in mM): 105 K-gluconate, 30 KCl, 10 HEPES, 10 phosphocreatinine, 4 ATP-Mg, 0.3 GTP-tris, and 0.3 EGTA, adjusted to pH 7.3 with KOH (285–290 mOsm). Micropipette position was controlled using a 3D micromanipulator (Burleigh PCS-PS60). Whole-cell patch clamp experiments were performed on n = 27 (soft surfaces) and n = 31 (stiff surfaces) neuronal networks using a total of 8 different cultures.

Constant negative pressure was applied to form the seal (>1GΩ) and whole-cell configuration of patch-clamp was achieved by gentle suction under voltage-clamp at −65 mV. Recordings were acquired with Axopatch-200A amplifier (Axon Instruments), low pass filtered at 1 kHz, digitized at 20 kHz with NI PCIe-6341 data acquisition board (National Instruments), stored and analyzed on a computer using WinLTP software [16]. Series resistance and cell capacitance were not compensated. Passive cellular parameters were extracted in voltage-clamp mode by analyzing current relaxation induced by a 10 mV hyperpolarizing step from the holding potential of −65 mV. Membrane potential was measured in normal current-clamp mode, immediately upon break-in. Only data from cells showing a membrane potential inferior to −50 mV and a membrane input resistance comprised between 190 and 500 MΩ were retained for further analysis. Action potential firing was analyzed from current-clamp recordings. Intrinsic excitability was investigated by injecting a 500 ms hyperpolarizing step current pulse of −40 pA followed by a 500 ms depolarizing step current pulse ranging from 0 to 200 pA with 10 pA increments. The number of action potentials was counted up on each depolarizing step. The presence of miniature synaptic currents was assessed under voltage-clamp at −65 mV over 1-min recordings.

2.10. Statistical analysis

We used a total number of 17 different cultures of primary rat cortical neurons (RCN) that were prepared from the cortex of day-18 rat embryos (Life Technologies, Gaithersburg, MD). Each culture corresponds to approximately 1.3 million cortical neurons obtained from 2 day to 18 rat embryos. Fluorescent images presented in Figs. 2–4 and 6 were obtained from the average of different areas ($14 \leq n \leq 18$) of neuronal networks obtained from at least 8 different neuronal cultures. The quantification of the ratio of synapsin area to tubulin area presented in Fig. 6 was performed on n = 16 (soft surfaces) and n = 15 (stiff surfaces) neuronal networks using 5 different cultures. Whole-cell patch clamp experiments were performed on n = 27 (soft surfaces) and n = 31 (stiff surfaces) neuronal networks using 8 different cultures. Differences in means between groups were evaluated by two-tailed Student's t-tests performed in Origin 8.5 (OriginLab, Northampton, MA). For multiple comparisons the differences were determined by using an analysis of variance (ANOVA) followed by Tukey post-hoc test. $^{*}p < 0.05$, $^{*}p < 0.01$ and $^{***}p < 0.001$. Unless otherwise stated, all data are presented as mean ± standard deviation (S.D.).

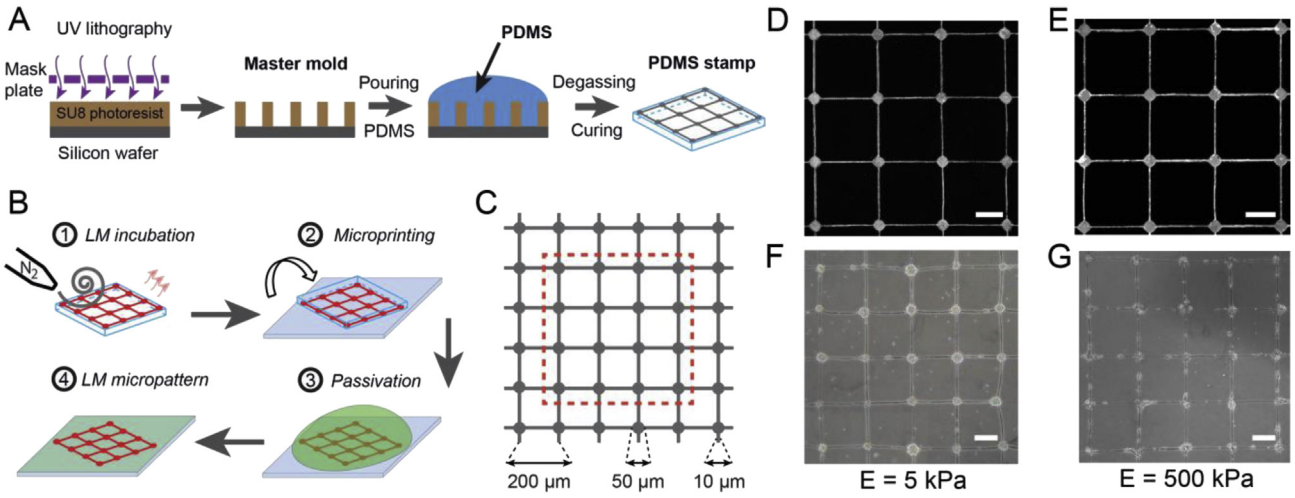

Fig. 1. (A) Soft lithography techniques were used to prepare microstamps in polydimethylsiloxane (PDMS). (B) PDMS microstamps were incubated with a solution of poly-L-lysine (PLL) and laminin (LM), dried with nitrogen and stamped to obtain (C) well-defined LM networks on (D) soft hydroxy-PAAm hydrogels (E = 5 kPa) and (E) stiff PDMS surfaces (E = 500 kPa). DIC images of neuronal networks obtained at DIV9 after the growth of RCN on (F) soft and (G) stiff microprinted surfaces.

3. Results

3.1. Protein micropatterns guide neuronal assembly

A standard photolithographic technique was used to create microstructured silicon masters that were molded in polydimethylsiloxane (PDMS) using Sylgard 184 silicone elastomer (Dow Corning, Midland, MI) to obtain PDMS microstamps (Fig. 1A). A solution of poly-L-lysine (PLL) and laminin (LM) was incubated during 1 h on the structured side of the PDMS microstamps, which were then dried with pure nitrogen (Fig. 1B). Inked PDMS microstamps were gently deposited on hydroxy-PAAm hydrogels (5.0 ± 0.3 kPa) and PDMS elastomers (508 ± 16 kPa), that exhibited a 100-fold difference in Young's modulus. Previous reports have indicated that brain tissue has an elastic modulus of 0.1–5 kPa [17,18]. We used 5 kPa hydroxy-PAAm hydrogels as our brain-like stiffness, whereas 500 kPa PDMS allows to obtain a 100-fold difference in Young's modulus in order to investigate the role of the matrix rigidity. We referred to hydroxy-PAAm and PDMS substrates from here onwards as the "soft" and "stiff" substrates, respectively. Uncoated zones on soft surfaces were passivated one night at 4 °C in a Bovine Serum Albumine (BSA) solution, whereas stiff surfaces were passivated one hour in a 1% Pluronic F-127 solution (Fig. 1B) to confine cell spreading and outgrowth on the printed grid pattern. LM micropatterns were composed of a network of circular islands of 50 μm in diameter connected with lines of 200 μm long and 10 μm width (Fig. 1C). As shown in Fig. 1D and E, LM micropatterns were transferred with high fidelity on either soft or stiff surfaces, respectively. Both micropatterned surfaces permitted to impose the assembly of cortical neurons that lead to a precise engineering of the neuronal network architecture on soft and stiff substrates (Fig. 1F and G) with accumulated neurons on the circular islands at DIV9.

Protein densities in micropatterns deposited on soft (Fig. 1D) and stiff (Fig. 1E) matrices were determined by immunofluorescence detection. We found a constant fluorescence intensity level across the different substrates indicating uniform distribution of ligand density and no statistical differences of protein density were found between soft and stiff matrices (Fig. S1). In addition, previous reports have shown that primary cortical neurons formed vinculin containing cell-substrate adhesions on soft hydroxy-PAAm and stiff PDMS substrates with similar areas [19], suggesting that neurons interact similarly with both substrates.

Single cortical neurons were plated on microprinted stiff PAAm (E~425 kPa) and stiff PDMS (E~500 kPa) substrates and then immunostained at DIV4 for Tau (axon), MAP-2 (neurite) and DAPI (nucleus). The axonal length was then quantified to control whether the nature of the culture substrate affect the axonal growth. We found that the axonal length of monopolar and bipolar cortical neurons was statistically similar at DIV4 on stiff PAAm and PDMS substrates (Fig. S2), supporting that the growth of axons is not affected on PAAm and PDMS substrates with similar stiffness and biochemical coatings. Taken together these results suggest that cortical neurons will be only sensitive to differences in matrix stiffness between soft hydroxy-PAAm and stiff PDMS substrates.

Assuming that cortical neurons were homogeneously plated on LM micropatterns at DIV0, the migration of individual neurons on LM tracks is the most obvious hypothesis to explain the accumulation of neurons on the circular islands. To verify this hypothesis, we have quantified the dynamics of neuron assembly on stiff and soft micropatterned substrates.

3.2. Neuronal network assembly on stiff substrates

Primary cortical neurons were plated at 50.000 cells/cm^2 on stiff microprinted substrates (E = 508 ± 16 kPa), observed in differential interference contrast (DIC) mode (Fig. 2A) then fixed and immunostained for actin (Fig. 2B), βIII-tubulin (Fig. 2C) and DAPI (Fig. 2D) at DIV0, DIV4, DIV9 and DIV15. As expected, cortical neurons were homogeneously distributed on LM micropatterns at DIV0 (Fig. 2A and D) and our results showed that neurons started to accumulate on circular islands from DIV4. Importantly, the topological confinement of cortical neurons on the grid micropattern was preserved for up to 21 days *in vitro* on stiff substrates (Fig. S3).

We then determined the spatial distribution of actin, βIII-tubulin and DAPI by averaging and color-coding epifluorescence images of similar zones of different cortical networks. These zones were composed of 9 circular islands of 50 μm in diameter and 12 linear tracks of 200 μm long and 10 μm width. Averaged immunostained images indicated that actin was gradually concentrated on the circular islands to reach a maximal intensity at DIV15 (Fig. 2B), whereas the actin fluorescent signal was very low in the linear tracks. In the contrary, an intense βIII-tubulin fluorescent signal was found both on circular islands and linear tracks from

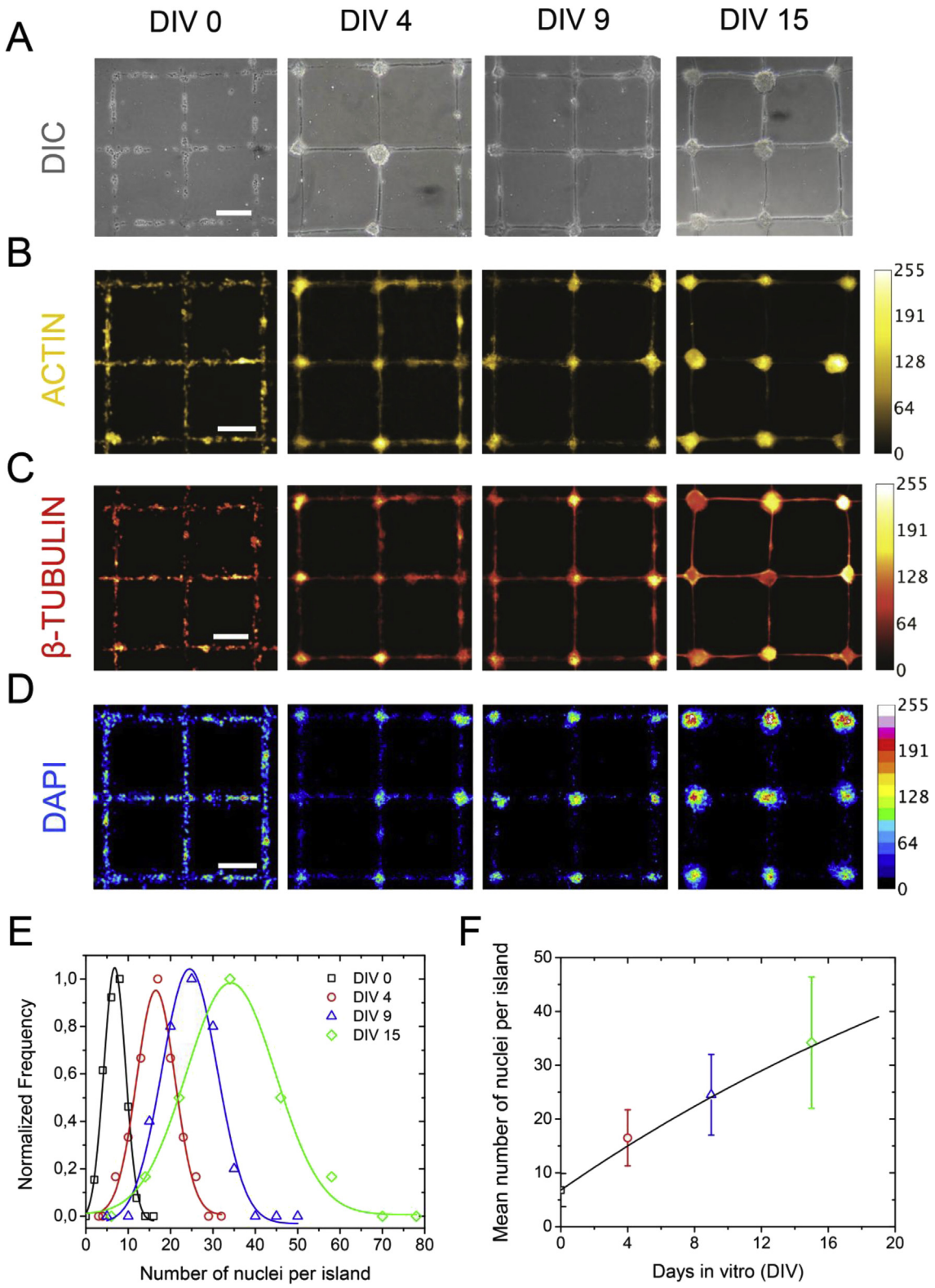

Fig. 2. The formation of neuronal networks on stiff microprinted elastomers (E = 500 kPa) was observed at DIV0, DIV4, DIV9 and DIV15 with (A) differential interference contrast (DIC) microscopy. Fluorescent images of the average distribution of (B) F-actin (n = 14), (C) ßIII-tubulin (n = 16) and (D) nuclei staining with DAPI (n = 16). Scale bars are 100 μm. (E) Representation of the normalized frequency as a function of the number of nuclei per island for DIVO, DIV4, DIV9 and DIV15. The total number of nuclei is n = 68 (DIV0, in black), n = 81 (DIV4, in red), n = 72 (DIV9, in blue) and n = 71 (DIV15, in green) and correspond to 9 different cultures. (F) The mean number of nuclei (Mean ± S.D.) per circular island increased linearly with time on stiff substrates. Mean ± S.D. were obtained from (E) and resulted from the quantification of $10 \leq n \leq 12$ different areas of neuronal networks for each DIV using a total number of 9 cultures. (For interpretation of the references to colour in this figure legend, the reader is referred to the web version of this article.)

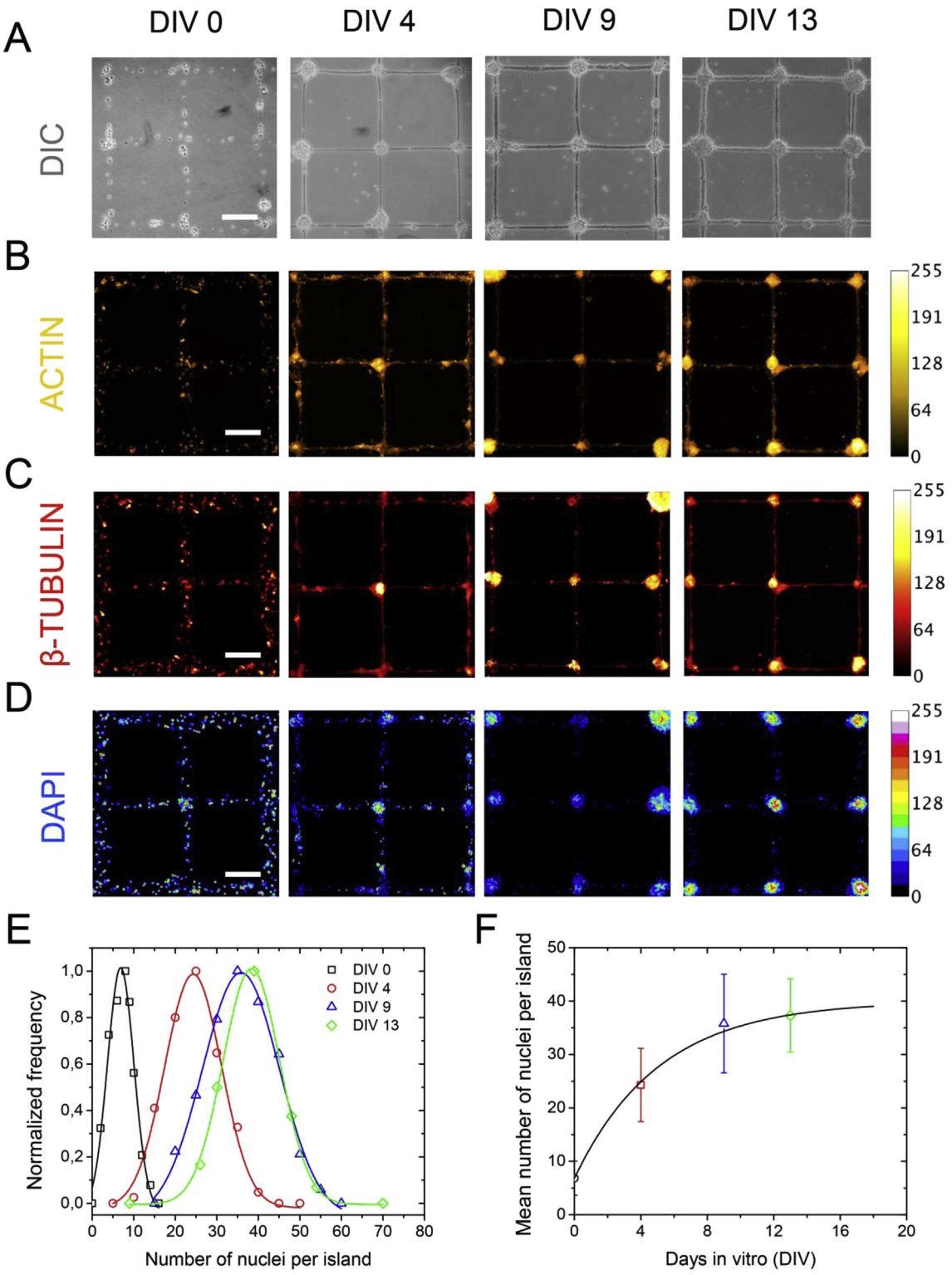

Fig. 3. (A) Sequence of DIC images of the formation of cortical neuronal networks on soft microprinted hydrogels (5 kPa) at DIV0, DIV4, DIV9 and DIV13. Fluorescent images of the average distribution of (B) F-actin (n = 9), (C) ßIII-tubulin (n = 15) and (D) nuclei staining with DAPI (n = 14). Scale bars are 100 μm. (E) Representation of the normalized frequency as a function of the number of nuclei per island for DIVO, DIV4, DIV9 and DIV13. The total number of nuclei is n = 63 (DIV0, in black), n = 76 (DIV4, in red), n = 82 (DIV9, in blue) and n = 81 (DIV15, in green) and correspond to 9 different cultures. (F) The mean number of nuclei (Mean ± S.D.) per circular island increased non-linearly with time on soft substrates. (For interpretation of the references to colour in this figure legend, the reader is referred to the web version of this article.)

DIV9 (Fig. 2C), suggesting that neurites grown on LM lines. High-magnification images indicated the tubulin signal at DIV0 is related to the formation of small processes (Fig. S4), whereas fasciculated processes that formed a bundle of packed extensions were observed on both substrates at DIV4. DAPI immunostained images confirmed that nuclei were homogeneously distributed on the grid micropattern at DIV0 and then gradually accumulated on circular islands, as demonstrated by the high level of DAPI

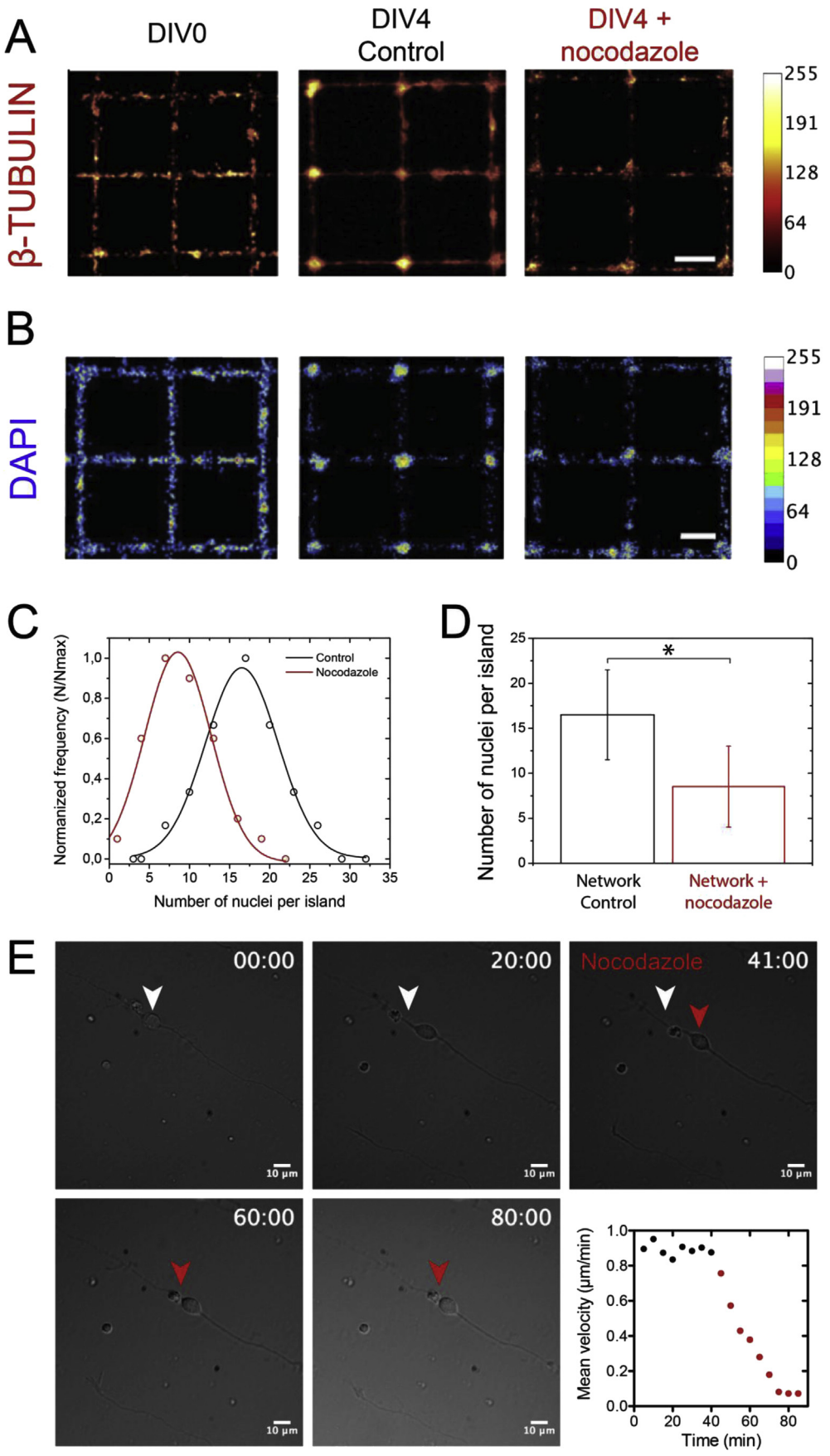
A
DIV0
DIV4
Control
DIV4 +
nocodazole
β-TUBULIN
255
191
128
64
0
B
DAPI
255
191
128
64
0
C
Normanized frequency (N/Nmax)
Number of nuclei per island
Control
Nocodazole
D
Number of nuclei per island
*
Network
Control
Network +
nocodazole
E
00:00
20:00
Nocodazole
41:00
60:00
80:00
10 µm
Mean velocity (µm/min)
Time (min)

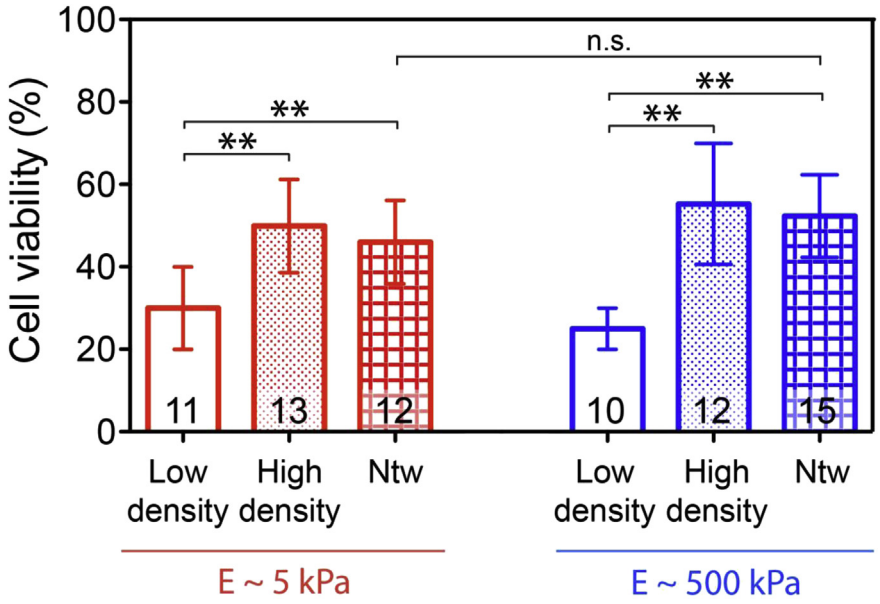

Fig. 5. Evolution of the cell viability obtained from live/dead assays at DIV13 on cortical neurons grown on soft low cell-density (white bars), high cell-density (dotted bars) and micropatterned networks (dashed bars) on soft (5 kPa, in red) and stiff (500 kPa, in blue) matrices. The number of samples used for cell viability assays is indicated at the bottom of the bars and correspond to a total number of 6 cultures. (For interpretation of the references to colour in this figure legend, the reader is referred to the web version of this article.)

fluorescence observed at DIV15 in circular islands (Fig. 2D). By combining the threshold of fluorescent DAPI images with confocal imaging, we next quantified the number of nuclei per circular island from DIV0 to DIV15 (Fig. 2E). Our results showed that the number of nuclei increased linearly to reach a final value of 34 ± 9 nuclei per circular island at DIV15.

3.3. The formation dynamics of neuronal networks is enhanced on soft substrates

A similar density of cortical neurons (50,000 cells/cm^2) was deposited on soft micropatterned substrates (5.0 ± 0.3 kPa) and observed with DIC (Fig. 3A) and fluorescent microscopy (Fig. 3B–D). As observed on stiff substrates, cortical neurons were homogeneously distributed at DIV0 and started to accumulate in circular islands from DIV4 (Fig. 3A and D), whereas actin was concentrated in circular islands (Fig. 3B) and ßIII-tubulin was found both in linear tracks and circular islands (Fig. 3C). Contrary to stiff substrates, the topological confinement of cortical neurons on the grid micropattern was only preserved for 13 days *in vitro*. Indeed, cortical neuronal networks formed on soft substrates showed the formation of thick neurite bundles (Fig. 3A) with accumulated tension that often lead to the formation of topological defects after DIV13 (Fig. S5). To better characterize this phenomenon, we measured on DIC images at DIV13 the inter-island distances (from center to center) of neuronal networks grown on soft PAAm substrates (Fig. S6). We obtained a mean inter-island distance of 200.8 ± 1.4 μm in controls (n = 26) and 154.7 ± 3.8 μm in networks with topological defects (n = 17), suggesting a mean contraction of ~23% at DIV 13 in approximately 65% of the neuronal networks.

We next quantified the normalized frequency as a function of the number of nuclei per island for DIVO, DIV4, DIV9 and DIV13 (Fig. 3E) to determine the impact of soft matrices on the dynamics of neuronal network assembly. By comparing our results on soft matrices (Fig. 3F) with those obtained on stiff matrices (Fig. 2E and F), we showed that nuclei accumulated faster on circular islands microprinted on soft substrates (n = 36 ± 9 at DIV9). Taken together, our results suggest that soft substrates accelerate the formation dynamics of oriented neuronal networks.

3.4. Cell migration drives the formation of neuronal networks

Our results show that the assembly of neuronal networks is faster on soft substrates and suggest that the motility of cortical neurons is enhanced by decreasing the matrix stiffness. To confirm that the motility of neurons is the driving process of the accumulation of cell bodies on circular islands, we used nocodazole to depolymerize microtubules [15] at early stages of the network assembly. Indeed, previous works have shown that the migration process of neurons, called *nucleokinesis*, critically depends on the microtubules network that surrounds the nucleus [20,21]. Nucleokinesis corresponds to the movement of the nucleus towards the cell body during neuronal migration in response to the movement of the centrosome.

Nocodazole was added at 0.3 nM in the culture media everyday between DIV0 and DIV3. Averaged fluorescent images of ßIII-tubulin indicate a lower fluorescence signal in circular islands for nocodazole-treated networks (Fig. 4A), suggesting that a significant part of the microtubule network was depolymerized. Interestingly, DAPI staining of nocodazole-treated networks showed a lower fluorescence intensity in circular islands at DIV4 comparing to controls and a higher fluorescence intensity on the linear tracks (Fig. 4B). Fluorescence observations suggest that cortical neurons with a disrupted microtubule network are less accumulated in

Fig. 4. Epifluorescent images of the average distribution of (A) βIII-tubulin (n = 16) and (B) nuclei staining with DAPI at DIV0 (n = 18), DIV4 (n = 18) and DIV4 + nocodazole (n = 18). Scale bars are 100 μm. (C) Representation of the normalized frequency as a function of the number of nuclei per island at DIV4 (in black, n = 18) and DIV4 with nocodazole treatment (in red, n = 14). (D) The mean number of nuclei per island was significantly lower at DIV4 in the presence of nocodazole. (E) Sequence of DIC images that show the cell body migration of a bipolar cortical neuron plated on a micropatterned stiff substrate. White and red arrows indicate the position of the cell body at t = 0 and t = 40 min, respectively. The culture media was replaced with a fresh media containing nocodazole at 0.9 nM at t = 40 min. The temporal evolution of the mean cell body velocity is plotted in black (t ≤ 40 min) and red (t > 40 min). (For interpretation of the references to colour in this figure legend, the reader is referred to the web version of this article.)

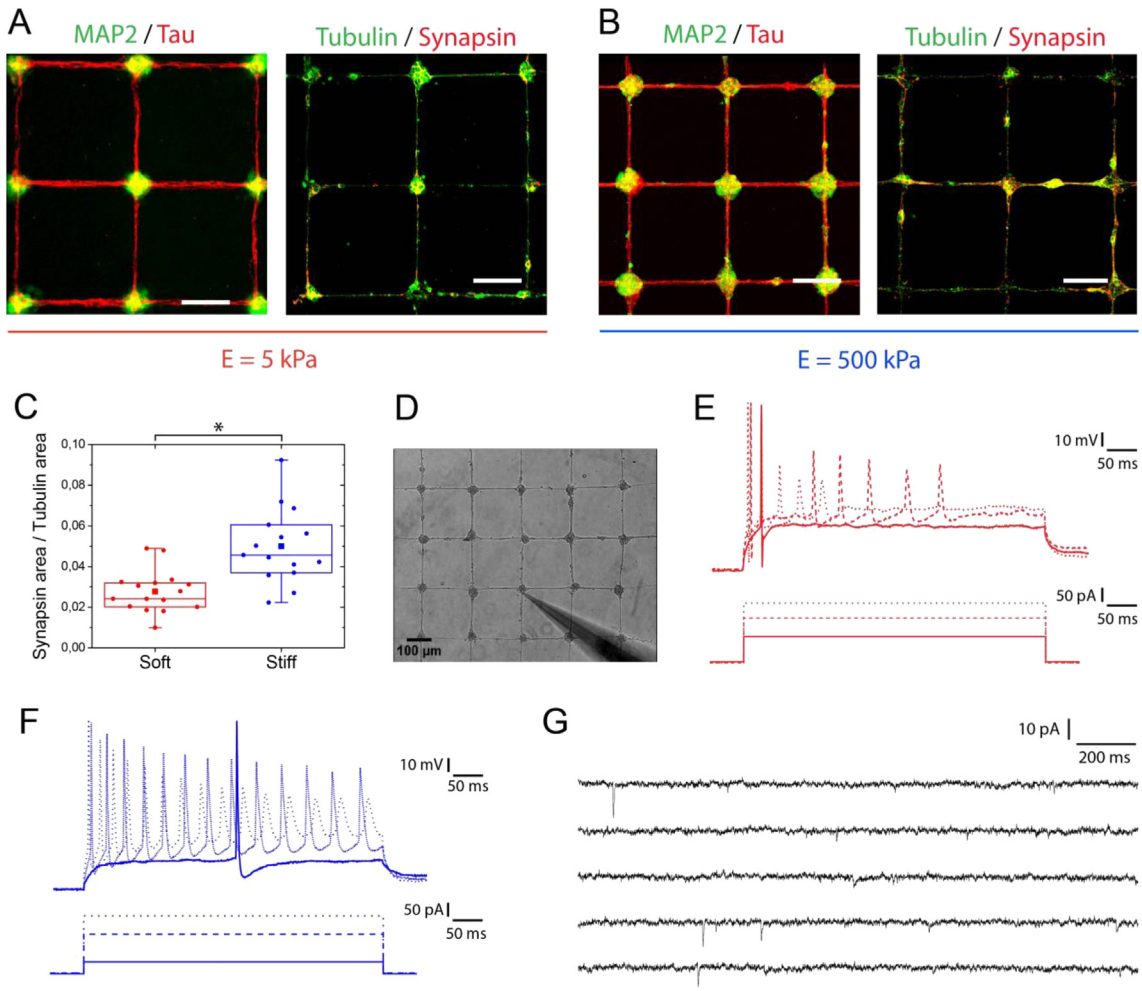

Fig. 6. Epifluorescent images of cortical neuronal networks grown on (A) soft and (B) stiff surfaces and immunostained for MAP2/Tau (DIV9) and βIII-tubulin/synapsin (DIV13). MAP2/Tau are averaged images obtained from different areas (soft: n = 14 and stiff: n = 12) using a total of 5 different cultures. Scale bars are 100 μm. (C) Quantification of the ratio of synapsin area to tubulin area for neuronal networks grown on soft (n = 16) and stiff matrices (n = 15) using 5 different cultures. (D) Phase contrast image of a typical patch clamp experiments performed on a micropatterned neuronal network. The scale bar is 100 μm. Action potential firing was analyzed from current-clamp recordings on (E) soft and (F) stiff matrices. Intrinsic excitability was investigated by injecting a 500 ms hyperpolarizing step current pulse of −40 pA followed by a 500 ms depolarizing step current pulse ranging from 0 to 200 pA with 10 pA increments. The number of action potentials was counted up on each depolarizing step. (G) Typical example of miniature synaptic currents were recorded in neuronal networks grown on stiff surfaces under voltage-clamp at −65 mV over 13 s.

circular islands than control cells. We next quantified the number of nuclei per island (Fig. 4C) in control and nocodazole-treated neurons at DIV4 and we found that the mean number of nuclei per island was two times lower in nocodazole-treated networks (Fig. 4D).

We then performed time-lapse experiments of neuronal migration at DIV4 to obtain direct evidence of the role of nocodazole in neuronal migration. Single cortical neurons were plated at low density on laminin micropatterns and the migration of the cell body was recorded with time-lapse microscopy in DIC mode during 40 min. Then, the culture media was replaced with a fresh media containing nocodazole at 0.9 nM and the migration was followed during a second period of 40 min (Movie S1). As shown in Fig. 4E, we observed a constant migration velocity of ~0.91 ± 0.17 μm/min during the first 40 min and then a slowing down of the migration velocity in response to nocodazole treatment that lead to a final migrating velocity of ~0.07 μm/min.

Altogether, our findings confirm that the microtubule network is an active player in the migration mechanism of cortical neurons and demonstrate that cell migration drives the formation of cortical neuronal networks in grid micropatterns through accumulation of cell bodies in circular islands.

3.5. Oriented neuronal networks enhance cell survival on soft and stiff matrices

To provide a quantitative measure of the health of cortical neuronal networks on soft and stiff matrices, we then quantified the cell viability with live/dead assays. Cell viability at DIV13 in patterned neuronal networks was compared with viability in low and high cell-density cultures to estimate the role of cell–cell interactions on cell survival. Assuming ~35 neurons per circular island at DIV 13 on soft and stiff matrices (Fig. 2F and G), we plated 1,75 millions of cells per cm^2 in high cell-density cultures to obtain identical culture conditions with micropatterned networks, whereas low cell-density cultures corresponded to the initial plating density at DIV0 of 50,000 cells per cm^2. As shown in Fig. 5, we found that the cortical neuronal viability increased significantly between low and high cell-density cultures on soft (51.4 ± 3.8%) and stiff (57.6 ± 5.0%) matrices, suggesting that forcing cell–cell interactions promotes cell viability. Interestingly, we observed that the cell viability of neuronal networks grown on soft (48.7 ± 8.6%)

and stiff (51.7 ± 8.1%) matrices was similar to high cell-density cultures (Fig. 5), demonstrating that oriented networks present optimal culture conditions for neuron viability.

Taken together, our findings indicate that oriented cortical networks promote the cell survival on soft and stiff matrices, whereas a 100-fold increase in substrate stiffness does not affect cell viability.

3.6. *Stiff substrates promote the formation of synaptic vesicles and enhance the electrophysiological activity of neuronal networks*

Cortical neurons on soft and stiff substrates were immunostained at DIV9 with anti-MAP2 and anti-Tau antibodies to label dendritic and axonal neurites on soft and stiff matrices, respectively (Fig. 6A and B). Averaged images (n = 9) presented in Fig. 6A and B showed that dendrites (MAP2 in green) were localized on circular islands, whereas axonal extensions (Tau in red) were observed on the linear tracks, regardless the matrix stiffness. These results confirm that axons of 200 μm length connect cell bodies accumulated on the circular islands in mature neuronal networks (DIV9) and suggest therefore that neuronal networks grown on stiff or soft matrices can propagate action potentials.

To test this hypothesis, we first assessed the presence of presynaptic connections at DIV15. Cortical networks grown on soft and stiff matrices were stained with ßIII-tubulin and synapsin, which is an abundant synaptic vesicle protein used as a marker of presynaptic terminals [22]. Synapsin was characterized on soft (Fig. 6A) and stiff (Fig. 6B) substrates by discrete points localized along neurites and on the soma. By thresholding fluorescent images, we estimated the ratio between the area of synapsin puncta and the total βIII-tubulin area for soft and stiff surfaces. As shown in Fig. 6C, we found that stiff matrices enhance significantly the synapsin to βIII-tubulin ratio, suggesting that stiff surfaces promote the formation of synaptic vesicles in cortical neuronal networks.

We then used the whole-cell patch clamp technique to assess the action potential firing from current-clamp recordings on networks grown on soft (n = 27) and stiff (n = 31) surfaces. Based on severe selection criteria (see the method section), we obtained successful whole-cell recordings for 5 neurons on soft surfaces and 12 neurons on stiff surfaces. Considering that maximum 2 attempts at whole-cell patch clamping could be made per networks due to neurons lifetime in the incubation chamber, the success rate was lower on soft matrices (9.3 ± 0.4%) than on stiff matrices (19.4 ± 0.7%). Resting membrane potential and membrane input resistance were not different between soft (−60 ± 4 mV and 344 ± 107 MΩ, respectively) and stiff substrates (−61 ± 6 mV and 375 ± 90 MΩ). The intrinsic excitability of neurons was investigated by injecting a 500 ms hyperpolarizing step current pulse of −40 pA followed by a 500 ms depolarizing step current pulse ranging from 0 to 200 pA with 10 pA increments. The number of action potentials was counted up on each depolarizing step. Our results show that the mean maximal number of action potentials was lower on soft matrices (Fig. 6E, n = 4 ± 3) than on stiff matrices (Fig. 6F, n = 12 ± 4), suggesting that the intrinsic excitability of cortical neurons is enhanced on stiff matrices. Membrane potential threshold for triggering the first action potential was similar on soft (−31 ± 1 mV) and stiff (−30 ± 6 mV) surfaces. Interestingly, we only observed the presence of miniature synaptic currents on stiff surfaces (Fig. 6G), confirming that matrix stiffness modulates the electrophysiological activity of cortical neurons.

4. Discussion

We report in this work a robust and very accessible way to produce mature neuronal cortical networks with a controlled architecture on different matrix stiffnesses. Indeed, microprinted neuronal networks was already achieved successfully on different surfaces such as glass [8,9], silicon substrates [23] or single-layered graphene substrates [24] but the effect of the surface rigidity on neuronal networks remained unknown. Here we show that cortical neuronal networks designed on stiff substrates maintained their spatial structures for up to 21 days *in vitro* without altering their spatial organization and functional activity, allowing to investigate the basic principles of the physical and functional connectivity within large neuronal networks. Well-controlled neuronal networks are obtained *in vitro* by controlling the spontaneous migration of cortical neurons with adhesive micropatterns. By confining soma location and neurite elongation to a predefined pattern, our method opens a way to generate reproducible and standardized neuronal networks that would facilitate the study of the interactions of individual neurons with their neighbors or the behavior of neuronal networks after incubation with pharmacological agents. In addition, the versatility of soft lithography allows to design a wide diversity of patterns to organize pluricellular networks while controlling the number of cell interactions.

Our findings show that soft matrices lead to a faster assembly of cell bodies on the circular patterns deposited on soft substrates, suggesting that matrix stiffness modulates the migration speed of cortical neurons. This hypothesis is in agreement with the repeatedly observed but still controversially discussed 'inverse' or 'negative' mechanotaxis of neurons [25–27]. In this context, Koch and coworkers showed that neurites from DRG neurons display maximal outgrowth on substrates with a Young's modulus of ~1000 Pa, whereas hippocampal neurite outgrowth is independent of substrate stiffness [28]. Together, these results underline that mechanosensitivity depends on neuronal cell type and may be modulated by external factors. While inverse mechanotaxis was only observed for neurons, Ueki and coworkers recently reported a similar phenomenon for fibroblasts in response to variations of the curvature of the elasticity boundary [29], suggesting that additional investigations are required to gain a more complete understanding of the conditions required to manipulate mechanotaxis.

Interestingly, our study demonstrates that cortical neurons can not only sense mechanical cues from their microenvironment, but also integrate these parameters into synapse connectivity and electrophysiological activity. Indeed, our results indicate that the synaptic density in cortical neuronal networks is enhanced on stiff substrates, whereas networks on soft substrates are characterized by a lower number of action potentials. Our findings are consistent with the recent report of Zhang and coworkers that suggests that stiff substrates significantly up-regulate Ca^{2+} signaling mechanisms in hippocampal neurons and enhance their synaptic connectivity as well as their excitatory synaptic transmission [30]. The dynamics of neural circuits arise through a complex interplay between synaptic inputs and the intrinsic electrical properties of individual neurons. The plasticity in the intrinsic excitability of cortical neuronal networks that was measured with polarizing steps (Fig. 6E–G) depends on the network activity and thus on synaptic inputs. In this context, one can assume that the more there are excitatory synapses, the more the intrinsic excitability of the network decreases [31]. This phenomenon allows a homeostatic regulation of the neuronal excitability that refers to the collective phenomena by which neurons alter their intrinsic or synaptic properties to maintain a target level of electrical activity. Taken together, our results support the hypothesis of an intrinsic mechanosensing mechanism in neurons that modulates their functional activity.

It is worth pointing out that contrary to other reports our cortical neuronal preparation contains a negligible amount of glial cells that permit to exclude their role in the mechanosensing

mechanism of cortical neurons. Despite recent investigations on transmembrane integrin proteins [19,32], RhoA [33], glutamate receptors [4] and specific ion channels [34], mechanotransduction in neurons is still poorly understood and further investigations will be required to understand this complex phenomenon. By using neuronal networks on compliant substrates, future work will focus on elucidating the role of the matrix stiffness on the balance of excitatory versus inhibitory receptors and the possible role for tension forces in neuronal and network function [35].

5. Conclusion

We envision that cortical neuronal networks of controlled architectures will be useful for studying in a reproducible and standardized way the mechanisms of brain injuries and degenerative diseases, as well as designing higher level of network complexity for neural engineering. In this context, future efforts could be made to combine micropatterned neuronal networks with multi-electrode array (MEA) recordings for achieving a long-term, non-invasive neuroelectronic interfacing. In addition, these results demonstrate the possibility to modulate the assembly dynamics and the functional activity of cortical neurons by tuning matrix stiffness and surface patterning. This approach is amenable to implementation on neural implants for controlling tissue–material interactions.

Acknowledgments

This work was supported by the Fonds National de la Recherche Scientifique F.R.S.-FNRS under Grants « Nanomotility » FRFC n° 2.4622.11 and « TIRF Microscopy » n° 1.5013.11F to S.G. and a European Research Council ERC Starting Grant ESKIN 259419 to S.P.L. Doctoral fellowships of J.L, D.M., C.B. and L.A. are supported by the Foundation for Training in Industrial and Agricultural Research (FRIA). The Mechanobiology and Soft Matter group belongs to the French research consortium GDR 3070 CellTiss.

Appendix A. Supplementary data

Supplementary data related to this article can be found at http://dx.doi.org/10.1016/j.biomaterials.2016.02.041.

References

[1] K. Franze, The mechanical control of nervous system development, Development 140 (2013) 3069–3077.
[2] P.C. Georges, W.J. Miller, D.F. Meaney, E.S. Sawyer, P.A. Jamney, Matrices with compliance comparable to that of brain tissue select neuronal over glial growth in mixed cortical cultures, Biophys. J. 90 (2006) 3012–3018.
[3] A.I. Teixeira, S. Ilkhanizadeh, J.A. Wigenius, J.K. Duckworth, O. Inganäs, O. Hermanson, The promotion of neuronal maturation on soft substrates, Biomaterials 30 (2009) 4567–4572.
[4] M.L. Previtera, C.G. Langhammer, N.A. Langrana, B.L. Firestein, Regulation of dendrite arborization by substrate stiffness is mediated by glutamate receptors, Ann. Biomed. Eng. 38 (2010) 3733–3743.
[5] M.C. Murphy, J. Huston, C.R. Jack Jr., K.J. Glaser, A. Manduca, J.P. Felmlee, et al., Decreased brain stiffness in Alzheimer's disease determined by magnetic resonance elastography, J. Magn. Reson. Imaging 34 (2011) 494–498.
[6] M.T. Prange, S.S. Margulies, Regional, directional, and age-dependent properties of the brain undergoing large deformation, J. Biomech. Eng. 124 (2002) 244–252.
[7] A. Gefen, N. Gefen, Q. Zhu, R. Raghupathi, S.S. Margulies, Age-dependent changes in material properties of the brain and braincase of the rat, J. Neurotrauma 20 (2003) 1163–1177.
[8] C. Wyart, C. Ybert, L. Bourdieu, C. Herr, C. Prinz, D. Chatenay, Constrained synaptic connectivity in functional mammalian neuronal networks grown on patterned surfaces, J. Neurosci. Methods 117 (2002) 123–131.
[9] E. Marconi, T. Nieus, A. Maccione, P. Valente, A. Simi, M. Messa, et al., Emergent functional properties of neuronal networks with controlled topology, PLoS One 7 (2012) e34648.
[10] J.W. Park, B. Vahidi, A.M. Taylor, S.W. Rhee, N.L. Jeon, Microfluidic culture platform for neuroscience research, Nat. Protoc. 1 (2006) 2128–2136.
[11] S. Dujardin, K. Lécolle, R. Caillierez, S. Bégard, N. Zommer, C. Lachaud, et al., Neuron-to-neuron wild-type Tau protein transfer through a trans-synaptic mechanism: relevance to sporadic tauopathies, Acta Neuropathol. Commun. 2 (2014) 14.
[12] M. Versaevel, T. Grevesse, M. Riaz, J. Lantoine, S. Gabriele, Micropatterning hydroxy-PAAm hydrogels and Sylgard 184 silicone elastomers with tunable elastic moduli, Micropatterning Cell Biol. Part C 121 (2014) 33–48.
[13] T. Grevesse, M. Versaevel, G. Circelli, S. Desprez, S. Gabriele, A simple route to functionalize polyacrylamide hydrogels for the independent tuning of mechanotransduction cues, Lab. Chip 13 (2013) 777–780.
[14] T. Grevesse, M. Versaevel, S. Gabriele, Preparation of hydroxy-PAAm hydrogels for decoupling the effects of mechanotransduction cues, J. Vis. Exp. (2014) 1–8.
[15] R.J. Vasquez, et al., Nanomolar concentrations of nocodazole alter microtubule dynamic instability in vivo and in vitro, Mol. Biol. Cell 8 (1997) 973–985.
[16] W.W. Anderson, G.L. Collingridge, Capabilities of the WinLTP data acquisition program extending beyond basic LTP experimental functions, J. Neurosci. Methods 162 (2007) 346–356.
[17] A.J. Engler, S. Sen, H.L. Sweeney, D.E. Discher, Matrix elasticity directs stem cell lineage specification, Cell 126 (2006) 677–689.
[18] I. Levental, P.C. Georges, P.A. Janmey, Soft biological materials and their impact on cell function, Soft Matter 3 (2007) 299–306.
[19] T. Grevesse, B.E. Dabiri, K.K. Parker, S. Gabriele, Opposite rheological properties of neuronal microcompartments predict axonal vulnerability in brain injury, Sci. Rep. 5 (2015) 9475.
[20] B.A. Samuels, L.H. Tsai, Nucleokinesis illuminated, Nat. Neurosci. 7 (2004) 1169–1170.
[21] L.H. Tsai, J.G. Gleeson, Nucleokinesis in neuronal migration, Neuron 46 (2005) 383–388.
[22] R. Llinás, J.A. Gruner, M. Sugimori, T.L. McGuinness, P. Greengard, Regulation by synapsin I and Ca2+-calmodulin-dependent kinase II of transmitter release in squid giant synapse, J. Physiol. 436 (1991) 257–282.
[23] C. Py, M. Martina, G.A. Diaz-Quijada, C.C. Luk, D. Martinez, M.D. Denhoff, et al., From understanding cellular function to novel drug discovery: the role of planar patch-clamp array chip technology, Front. Pharmacol. 2 (2011) 51.
[24] D. Hong, K. Bae, S. Yoo, K. Kang, B. Jang, J. Kim, et al., Generation of cellular micropatterns on a single-layered graphene film, Macromol. Biosci. 14 (2014) 314–319.
[25] P. Rauch, P. Heine, B. Goettgens, J.A. Käs, Forces from the rear: deformed microtubules in neuronal growth cones influence retrograde flow and advancement, New J. Phys. 15 (2013) 015007.
[26] K. Franze, J. Guck, The biophysics of neuronal growth, Rep. Prog. Phys. 73 (2010) 094601.
[27] L.A. Flanagan, Y.E. Ju, B. Marg, M. Osterfield, P.A. Janmey, Neurite branching on deformable substrates, Neuroreport 13 (2002) 2411–2415.
[28] D. Koch, W.J. Rosoff, J. Wang, H.M. Gekker, J.S. Urbach, Strength in the periphery: growth cone biomechanics and substrate rigidity response in peripheral and central nervous system neurons, Biophys. J. 102 (2012) 452–460.
[29] A. Ueki, S. Kidoaki, Manipulation of cell mechanotaxis by designing curvature of the elasticity boundary on hydrogel matrix, Biomaterials 41 (2015) 45–52.
[30] N.S. Desai, L.C. Rutherford, G.G. Turrigiano, Plasticity in the intrinsic excitability of cortical pyramidal neurons, Nat. Neurosci. 2 (1999) 515–520.
[31] Q.Y. Zhang, Y.Y. Zhang, J. Xie, C.X. Li, W.Y. Chen, B.L. Liu, et al., Stiff substrates enhance cultured neuronal network activity, Sci. Rep. 4 (2014) 6215.
[32] M.A. Hemphill, B.E. Dabiri, S. Gabriele, L. Kerscher, C. Franck, J.A. Goss, et al., A possible role for integrin signaling in diffuse axonal injury, PLoS One 6 (2011) e22899.
[33] L. Kam, W. Shain, J.N. Turner, R. Bizios, Axonal outgrowth of hippocampal neurons on micro-scale networks of polylysine-conjugated laminin, Biomaterials 22 (2001) 1049–1054.
[34] T. Kobayashi, M. Sokabe, Sensing substrate rigidity by mechanosensitive ion channels with stress fibers and focal adhesions, Curr. Opin. Cell. Biol. 22 (2010) 669–676.
[35] Amir Ayali, The function of mechanical tension in neuronal and network development, Integr. Biol. 2 (2010) 178–182.